Theoretical basis for interpreting heterodyne chirality-selective sum frequency generation spectra of water

Daniel Konstantinovsky[1,2,#,†], Ty Santiago[1,†], Matthew Tremblay[1], Garth J. Simpson[3], Sharon Hammes-Schiffer*[1,2], E. Chui-Ying Yan*[1]

[1]Department of Chemistry, Yale University, New Haven, Connecticut 06520, USA

[2]Department of Molecular Biophysics and Biochemistry, Yale University, New Haven, Connecticut 06520, USA

[3]Department of Chemistry, Purdue University, West Lafayette, Indiana 47907, USA

[#]Current Address: Department of Chemistry, Columbia University, New York, New York 10027, USA

[†]These authors contributed equally

*Corresponding authors

Email addresses: sharon.hammes-schiffer@yale.edu, elsa.yan@yale.edu

Keywords:

spectral fitting, vibrational coupling, chiral sum frequency generation spectroscopy

Data availability statement: The data that supports the findings of this study are available within the article and its supplementary material.

Abstract

Chirality-selective vibrational sum frequency generation spectroscopy (chiral SFG) has emerged as a powerful technique for the study of biomolecular hydration water due to its sensitivity to the induced chirality of the first hydration shell. Thus far, water O-H vibrational bands in phase-resolved heterodyne chiral SFG spectra have been fit using one Lorentzian function per vibrational band, and the resulting fit has been used to infer the underlying frequency distribution. Here, we show that this approach may not correctly reveal the structure and dynamics of hydration water. Our analysis illustrates that the chiral SFG responses of symmetric and asymmetric O-H stretch modes of water have opposite phase and equal magnitude and are separated in energy by intramolecular vibrational coupling and a heterogeneous environment. The sum of the symmetric and asymmetric responses implies that an O-H stretch in a heterodyne chiral SFG spectrum should appear as two peaks with opposite phase and equal amplitude. Using pairs of Lorentzian functions to fit water O-H stretch vibrational bands, we improve spectral fitting of previously acquired experimental spectra of model β-sheet proteins and reduce the number of free parameters. The fitting allows us to estimate the vibrational frequency distribution and thus reveals the molecular interactions of water in hydration shells of biomolecules directly from chiral SFG spectra.

Introduction

Spectral fitting has been a standard approach for extracting molecular information from vibrational spectra, including those obtained by chirality-sensitive vibrational sum frequency generation spectroscopy (chiral SFG). In recent years, chiral SFG has emerged as a powerful technique for studying the macromolecular hydration shell.[1-6] Few experimental techniques are able to probe water in biological hydration shells selectively. As a surface-selective technique, chiral SFG is able to resolve chirality at interfaces.[4, 7-13] Our group has shown that this technique is selective to the first hydration shell around a β-sheet protein.[2]

In general, data analysis of vibrational studies is performed by fitting vibrational spectra. Once a vibrational spectrum is fit, the central frequencies of each vibrational band give information as to the frequencies that are enriched in the vibrational density of states, which then lead to conclusions about the local environments of the vibrational modes of interest. However, recent computational modeling of heterodyne phase-resolved chiral SFG spectra has produced predictions that do not seem to fit the assumptions of this workflow. In particular, our group demonstrated that the isolated O-H stretch response of the first hydration shell around the β-sheet protein $LK_7\beta$ produces a characteristic "up-down" line shape (Figure 1a),[2, 14, 15] in contrast to the single peak of the infrared (IR) spectrum of the same ensemble of water (Figure 1b). It appears that the phase-resolved chiral SFG spectrum is not reporting directly the typical vibrational frequencies in the system. Thus, fitting the chiral SFG response of water with individual Lorentzian curves, as has been done so far, may not allow the estimation of the underlying vibrational frequency distribution reliably and therefore may fall short in revealing structures and dynamics of water in the protein hydration shell. Hence, our computational results call into question whether the application of the standard assumptions in analyzing chiral SFG signals from water in hydration shells of biomolecules is valid.

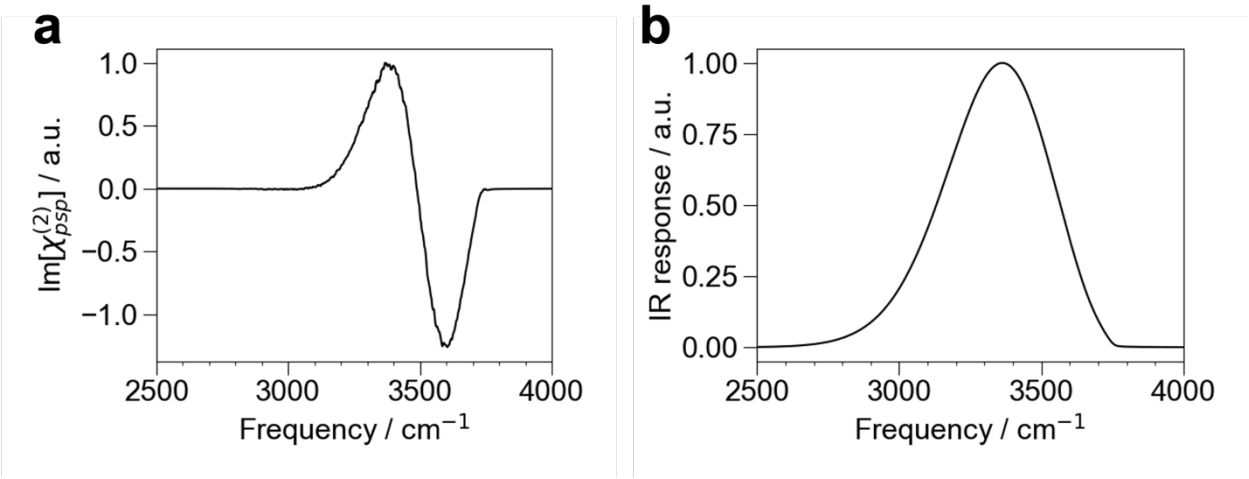

Figure 1. Simulated vibrational spectra of water in the first hydration shell around $LK_7\beta$. a) Chiral SFG (*psp*) response of water O-H stretch; b) IR response of the same water molecules, using the time-averaging approximation for a realistic peak width.[16] The spectrum in part a) was originally published in ref 2.

In this study, we demonstrate that the chiral SFG response of water around biomolecules is due to the incomplete cancellation of the responses of the symmetric and asymmetric stretching modes of water molecules. We show that the symmetric stretch response is the exact opposite of the asymmetric stretch response (Figure 2a). However, the symmetric and asymmetric stretch responses do not cancel because their frequencies are different due to intramolecular vibrational coupling and the variation in local environment of the two O-H groups within a single water molecule. Thus, their summation can lead to a nonzero "up-down" (or "down-up") chiral SFG signal (Figure 2b). This theoretical picture implies that the chiral SFG response of water provides an additional constraint to potentially improve curve fitting methods. Here, rather than fitting a separate Lorentzian curve to each O-H stretch feature, we fit water spectral responses with *pairs* of Lorentzian curves. Each pair of curves is with opposite phase, equal magnitude, and shifted frequencies. When applied to analyze our previously reported experimental chiral SFG spectra of β-sheet proteins,[2, 3, 14, 17] this fitting method allows us to reduce the number of free parameters and extract more reliable frequency distributions from spectra, hence directly revealing the distribution of local environments experienced by the O-H groups of water in the biomolecular hydration shell.

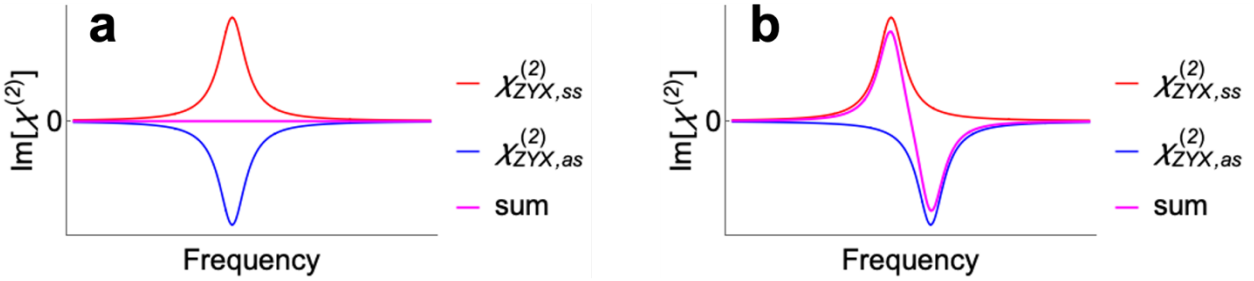

Figure 2. The origin of the chiral SFG line shape for the water O-H stretch. (a) Zero chiral SFG response in the absence of both intramolecular coupling and differences in the local environment of the two O-H groups. (b) An "up-down" line shape in the presence of coupling and a frequency difference between the symmetric and asymmetric stretches. Subscripts *ss* and *as* stand for the symmetric stretch and asymmetric stretch responses, respectively. See equation 2 for definition of $\chi^{(2)}_{ZYX}$, which is experimentally measured and computationally simulated to obtain chiral SFG spectra.

Theory

The chiral SFG signal arises from the molecular hyperpolarizability.

Vibrational SFG spectra are produced by overlapping in space and time an infrared (IR) beam and a visible beam at an interfacial sample and measuring the sum frequency output.[18] Under the electric dipole approximation, the response of the system arises solely from the optical electric fields, which are given by

$$\vec{E}_{\mathrm{SFG}} = E^{X}_{\mathrm{SFG}}\hat{X} + E^{Y}_{\mathrm{SFG}}\hat{Y} + E^{Z}_{\mathrm{SFG}}\hat{Z} \tag{1}$$

Where $\hat{X}$, $\hat{Y}$, and $\hat{Z}$ are unit vectors corresponding to each coordinate axis in the laboratory frame and E^{X}_{SFG}, E^{Y}_{SFG}, and E^{Z}_{SFG} are the components of the electric field vector. Chiral SFG measures elements of the nonlinear response tensor $\chi^{(2)}$, a third-order tensor, which is defined by

$$E^{I}_{\mathrm{SFG}} = \sum_{JK} \chi^{(2)}_{IJK} E^{J}_{\mathrm{vis}} E^{K}_{\mathrm{IR}} \tag{2}$$

where E^{J}_{vis} and E^{K}_{IR} are the components of the optical electric fields for the visible and IR beams, respectively, and *I*, *J*, and *K* range over the directions *X*, *Y*, and *Z*. The macroscopic $\chi^{(2)}$ emerges from an ensemble average of the microscopic molecular SFG response, the hyperpolarizability tensor β. For uniaxial interfacial assemblies, the orientation distribution in the azimuthal rotation angle ϕ can be assumed to be uniform, leading to

$$\chi^{(2)}_{IJK}(\theta,\psi) = \sum_n \frac{1}{2\pi} \int_0^{2\pi} d\phi_n \sum_{ijk} R^n_{Ii}(\phi_n,\theta_n,\psi_n) R^n_{Jj}(\phi_n,\theta_n,\psi_n) R^n_{Kk}(\phi_n,\theta_n,\psi_n) \beta^n_{ijk} \quad (3)$$

where β^n is the 27-element hyperpolarizability tensor of the n^{th} molecule in the system, i, j, and k range over the three-dimensional Cartesian coordinates (x, y, z) of the molecular frame, $\mathbf{R^n}$ is an Euler rotation matrix projecting the SFG response from the n^{th} molecular frame to the laboratory frame, and ϕ_n, θ_n, and ψ_n are the Euler angles of the n^{th} molecule projecting on to the laboratory coordinate (X, Y, Z). The molecular hyperpolarizability (β) arises from the Raman tensor ($\boldsymbol{\alpha}$) and the transition dipole ($\boldsymbol{\mu}$) of the n^{th} molecule according to[19,20]

$$\beta^n_{ijk} \propto \alpha^n_{ij} \mu^n_k \quad (4)$$

One of the surprising consequences of equation 3 is that some achiral chromophores exhibiting local mirror-plane symmetry in β may produce nonzero chiral $\chi^{(2)}$ elements, as outlined by the Simpson group.[12 13, 21] This serves as a theoretical basis for chiral SFG methods probing hydration structures of biomolecules because it implies that achiral water molecules arranged in chiral superstructures at interfaces can produce chiral SFG signals. Thus, chiral SFG can selectively probe the biomolecular hydration shell without interference from bulk water. By manipulating the polarization of the IR and visible beams and the polarization setting for detecting SFG signals, particular components of $\chi^{(2)}$ can be isolated. For example, the *psp* polarization measures the response from the elements $\chi^{(2)}_{ZYX}$, $\chi^{(2)}_{XYZ}$, $\chi^{(2)}_{ZYZ}$, and $\chi^{(2)}_{XYX}$,[9, 22] where p is polarization on the incident plane and s is polarization perpendicular to the incident plane, and the order of the subscript notation of *psp* is for the SFG, visible, and IR beams, respectively. Of the four elements, only $\chi^{(2)}_{ZYX}$ survives in a uniaxial system with C_∞ symmetry and in the absence of electronic resonance.[9] Hence, we measure $\chi^{(2)}_{ZYX}$ in our chiral SFG experiments under the conditions of electronic nonresonance and compute $\chi^{(2)}_{ZYX}$ to simulate chiral SFG spectra.

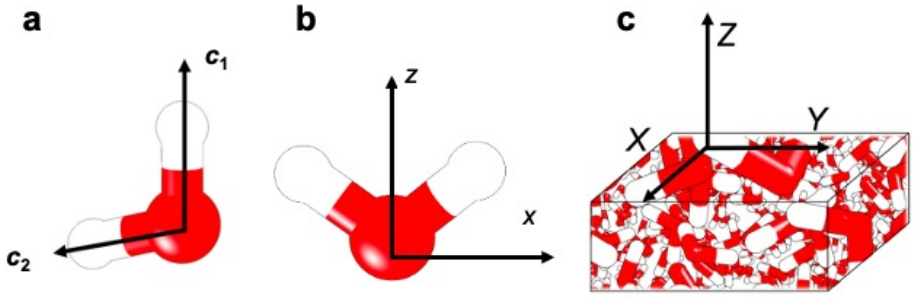

Figure 3. The four coordinate systems used in the derivation: (a) the two O-H frames (a_1, b_1, c_1) and (a_2, b_2, c_2), (b) the molecular frame (x, y, z), and (c) the laboratory frame (X, Y, Z).

The chiral SFG symmetric and asymmetric stretch responses are opposite in sign.

In order to validate the model that explains the "up-down" (or "down-up") line shape of the chiral SFG response of water as presented in Figure 2b, we must prove that 1) the symmetric and asymmetric stretches are at different frequencies, and 2) the symmetric and asymmetric stretches of water chiral SFG responses are equal but have opposite signs. Point 1 is known to be true, as intramolecular coupling and differences in the local environments of the two O-H groups in a water molecule cause the symmetric and asymmetric stretches to be non-degenerate. Therefore, we need to prove point 2:

$$\chi^{(2)}_{ZYX,\mathrm{ss}} = -\chi^{(2)}_{ZYX,\mathrm{as}} \tag{5}$$

where "ss" refers to the symmetric stretch and "as" to the asymmetric stretch. To do so, we define four frames of reference (Figure 3). They include two frames corresponding to two O-H groups: (a_1, b_1, c_1) and (a_2, b_2, c_2), one frame corresponding to the entire water molecule: (x, y, z), and the laboratory frame: (X, Y, Z). In the two O-H frames (Figure 3a), the corresponding c_1-axis and c_2-axis point along the O-H bonds. In the molecular frame (Figure 3b), the z-axis points along the bisector of the H–O–H angle and the x-axis is in the H–O–H plane. In the laboratory frame, the Z axis is perpendicular to the interface defining the uniaxial system and the X and Y axes point along the surface.

For water in the C_{2v} point group, the symmetric stretch corresponds to the A_1 irreducible representation and the asymmetric stretch corresponds to the B_1 irreducible representation for the coordinate system shown in Figure 3b. The corresponding elements of the molecular hyperpolarizability are $\beta^{zzz}_{H_2O}$, $\beta^{xxz}_{H_2O}$ and $\beta^{yyz}_{H_2O}$ for the symmetric stretch and $\beta^{xzx}_{H_2O}$ and $\beta^{zxx}_{H_2O}$ for the asymmetric stretch. In a uniaxial system of C_{2v} molecules, following equation 3, the chiral SFG response is given by[9, 12, 13, 15, 21]

$$\chi^{(2)}_{IJK} = \frac{1}{2}\sin^2\theta \sin\psi \cos\psi(-\beta^{xxz}_{H_2O} + \beta^{yyz}_{H_2O} + \beta^{xzx}_{H_2O}) \tag{6}$$

Therefore, the symmetric stretch contribution is

$$\chi^{(2)}_{IJK,ss} = \frac{1}{2}\sin^2\theta \sin\psi \cos\psi(-\beta^{xxz}_{H_2O} + \beta^{yyz}_{H_2O}) \tag{7}$$

and the asymmetric stretch contribution is

$$\chi^{(2)}_{IJK,as} = \frac{1}{2}\sin^2\theta \sin\psi \cos\psi(\beta^{xzx}_{H_2O}) \tag{8}$$

Relationships between these symmetric and asymmetric tensor contributions can be further simplified by considering the intramolecular coupling as a relatively minor perturbation to a system of two uncoupled local-mode O-H stretching motions. We can then express the molecular hyperpolarizability β elements in equation 6 in terms of the surviving hyperpolarizability elements in the two O-H frames illustrated in Figure 3a. Prior to "turning on" coupling, each of the individual O-H motions is linear (local C_∞-symmetry). Hence, the only surviving elements are β^{ccc}_{OHi} and $\beta^{aac}_{OHi} = \beta^{bbc}_{OHi}$, where i = 1 or 2 (Figure 3a). In this perturbation theoretical framework, the signs and magnitudes of the symmetric and asymmetric motions can be generated by projecting the local-mode O-H motions from the two separate O-H bond frames (a_1, b_1, c_1) and (a_2, b_2, c_2) (Figure 1a) to the water molecular frame (x, y, z) (Figure 3b). The first O-H frame is related to the molecular frame by the transformation matrix of

$$S_1 = \begin{pmatrix} \cos\theta' & 0 & \sin\theta' \\ 0 & 1 & 0 \\ -\sin\theta' & 0 & \cos\theta' \end{pmatrix} \tag{9}$$

where θ' = 52.25°, which is the angle between the c_1 axis and z axis (Figure 3), and half the water molecule's H–O–H angle. The second O-H frame is related to the molecular frame with an opposite direction of rotation by the transformation matrix of

$$S_2 = \begin{pmatrix} \cos\theta' & 0 & -\sin\theta' \\ 0 & 1 & 0 \\ \sin\theta' & 0 & \cos\theta' \end{pmatrix} \tag{10}$$

Hence, the molecular hyperpolarizability β_{H_2O} can be expressed in terms of β_{OH1} and β_{OH2}:

$$\beta^{ijk}_{H_2O} = S_1^{ii'} S_1^{jj'} S_1^{kk'} \beta^{i'j'k'}_{OH1} + S_2^{ii'} S_2^{jj'} S_2^{kk'} \beta^{i'j'k'}_{OH2} \tag{11}$$

where i, j, and k range over the molecular coordinates x, y, and z and i', j', and k' range over the OH bond coordinates a, b, and c. Thus, we can obtain

$$\begin{aligned} \beta^{yyz}_{H_2O} &= (S_1^{yc} S_1^{yc} S_1^{zc} \beta^{ccc}_{OH1} + S_2^{yc} S_2^{yc} S_2^{zc} \beta^{ccc}_{OH2}) \\ &+ (S_1^{ya} S_1^{ya} S_1^{zc} \beta^{aac}_{OH1} + S_2^{ya} S_2^{ya} S_2^{zc} \beta^{aac}_{OH2}) \\ &+ (S_1^{yb} S_1^{yb} S_1^{zc} \beta^{bbc}_{OH1} + S_2^{yb} S_2^{yb} S_2^{zc} \beta^{bbc}_{OH2}) \\ &= 0 + 0 + 0 + 0 + \cos\theta' \beta^{aac}_{OH1} + \cos\theta' \beta^{aac}_{OH2} \\ &= \cos\theta' (\beta^{aac}_{OH1} + \beta^{aac}_{OH2}) \end{aligned} \tag{12}$$

$$\begin{aligned} \beta^{xxz}_{H_2O} &= (S_1^{xc} S_1^{xc} S_1^{zc} \beta^{ccc}_{OH1} + S_2^{xc} S_2^{xc} S_2^{zc} \beta^{ccc}_{OH2}) \\ &+ (S_1^{xa} S_1^{xa} S_1^{zc} \beta^{aac}_{OH1} + S_2^{xa} S_2^{xa} S_2^{zc} \beta^{aac}_{OH2}) \\ &+ (S_1^{xb} S_1^{xb} S_1^{zc} \beta^{bbc}_{OH1} + S_2^{xb} S_2^{xb} S_2^{zc} \beta^{bbc}_{OH2}) \\ &= \sin^2\theta' \cos\theta' \beta^{ccc}_{OH1} + \sin^2\theta' \cos\theta' \beta^{ccc}_{OH2} \\ &+ \cos^3\theta' \beta^{aac}_{OH1} + \cos^3\theta' \beta^{aac}_{OH2} + 0 + 0 \\ &= \sin^2\theta' \cos\theta' (\beta^{ccc}_{OH1} + \beta^{ccc}_{OH2}) + \cos^3\theta' (\beta^{aac}_{OH1} + \beta^{aac}_{OH2}) \\ &= \sin^2\theta' \cos\theta' (\beta^{ccc}_{OH1} + \beta^{ccc}_{OH2}) + \cos\theta' (1 - \cos^2\theta') (\beta^{aac}_{OH1} + \beta^{aac}_{OH2}) \\ &= \sin^2\theta' \cos\theta' \left[(\beta^{ccc}_{OH1} + \beta^{ccc}_{OH2}) - (\beta^{aac}_{OH1} + \beta^{aac}_{OH2}) \right] + \cos\theta' (\beta^{aac}_{OH1} + \beta^{aac}_{OH2}) \end{aligned} \tag{13}$$

$$\begin{aligned} \beta^{xzx}_{H_2O} &= (S_1^{xc} S_1^{zc} S_1^{xc} \beta^{ccc}_{OH1} + S_2^{xc} S_2^{zc} S_2^{xc} \beta^{ccc}_{OH2}) \\ &+ (S_1^{xa} S_1^{za} S_1^{xc} \beta^{aac}_{OH1} + S_2^{xa} S_2^{za} S_2^{xc} \beta^{aac}_{OH2}) \\ &+ (S_1^{xb} S_1^{zb} S_1^{xc} \beta^{bbc}_{OH1} + S_2^{xb} S_2^{zb} S_2^{xc} \beta^{bbc}_{OH2}) \\ &= \sin^2\theta' \cos\theta' \beta^{ccc}_{OH1} + \sin^2\theta' \cos\theta' \beta^{ccc}_{OH2} \\ &+ \cos\theta' (-\sin\theta') \sin\theta' \beta^{aac}_{OH1} \\ &+ \cos\theta' \sin\theta' (-\sin\theta') \beta^{aac}_{OH2} + 0 + 0 \\ &= \sin^2\theta' \cos\theta' \left[(\beta^{ccc}_{OH1} + \beta^{ccc}_{OH2}) - (\beta^{aac}_{OH1} + \beta^{aac}_{OH2}) \right] \end{aligned} \tag{14}$$

Substituting equations 12-14 into equations 7 and 8 shows that the symmetric and asymmetric stretch signals from a water molecule are equal but opposite (equation 5). This statement is true whether or not the two O-H groups have equivalent hyperpolarizabilities, and thus it is applicable to water molecules in complex, heterogeneous environments.

This result seems to imply that the total chiral signal is zero. However, in reality, the symmetric and asymmetric signals are shifted in frequency relative to one another due to both vibrational coupling and heterogeneous local environments. The asymmetric component is typically assumed to have the higher frequency because the average intramolecular coupling is negative.[23] Hence, the symmetric and asymmetric responses do not perfectly cancel, and instead they produce a characteristic two-peak line shape (Figure 2b). This two-peak line shape can be "up-down" or "down-up". When the symmetric stretch response is positive and the asymmetric stretch is negative, the line shape will be "up-down" (Figure 2b), and vice versa for a "down-up" line shape.

Fitting experimental chiral SFG spectra with pairs of Lorentzian curves

The breakdown of the chiral SFG signal of individual water molecules into symmetric and asymmetric components implies that one needs to derive a new functional form to fit the heterodyne chiral SFG spectra of water. This will allow for extracting information about the underlying frequency distribution that can reveal molecular interactions of water. The functional form for a pair of water O-H stretching peaks should contain a pair of opposite Lorentzian curves with equal amplitude and a frequency displacement, as in

$$f(\omega) = \mathrm{Im}\left[\frac{A}{\omega - (\nu - \frac{1}{2}\Delta\nu) - i\Gamma} + \frac{-A}{\omega - (\nu + \frac{1}{2}\Delta\nu) - i\Gamma}\right] \tag{15}$$

where ω is the IR frequency, A is the amplitude of the pair, ν is the frequency of the midpoint between the two Lorentzian curves, $\Delta\nu$ is the difference in frequency between the two Lorentzian curves, and Γ relates to the peak width. This functional form involves fewer free parameters in fitting the chiral SFG spectra of water, as fitting two Lorentzian curves requires six parameters (two amplitudes, two widths, and two centers) whereas the new functional form requires only four (one amplitude, one width, center frequency, and a frequency difference). Fitting to a pair of opposite curves yields one center frequency instead of two, thus producing a single peak in the

frequency distribution, which is consistent with the IR spectrum of first hydration shell water (Figure 1).

The experimental spectra contain contributions of N-H stretches from the protein and O-H stretches from water. The water contributions can be described by the functional form in equation 15, while the protein contributions can be still described by individual Lorentzian functions. Hence, a linear combination of equation 15 for the water contributions and individual Lorentzian functions for the protein contributions can be used to fit the experimental spectra:

$$f(\omega) = \mathrm{Im}\left[\sum_m \frac{A_m}{\omega - \nu_m - i\Gamma_m}\right] + \mathrm{Im}\left[\sum_n \frac{A_n}{\omega - (\nu_n - \frac{1}{2}\Delta\nu_n) - i\Gamma_n} + \frac{-A_n}{\omega - (\nu_n + \frac{1}{2}\Delta\nu_n) - i\Gamma_n}\right] \quad (16)$$

where ν_n is the resonant frequency of the n^{th} pair of water peaks, ν_m is the resonant frequency of the m^{th} unpaired protein peak, A_n and A_m are the corresponding amplitudes, Γ_n and Γ_m are the corresponding damping coefficients, and $\Delta\nu_n$ is the difference in frequency for the n^{th} water symmetric and asymmetric stretches.

In fitting the experimental spectra, we assumed a known frequency difference between the symmetric and asymmetric stretches of water ($\Delta\nu$) to further constrain the fitting. Leaving $\Delta\nu$ as a free parameter of the fit often produced nonphysical results (e.g., $\Delta\nu$ values so large that the peaks in the pair were completely independent, or so small that the fit curve was flat due to cancelation of the two peaks that are equal in amplitude but opposite in sign). To address this issue, the initial value can be selected based on our theoretical studies. In principle, the $\Delta\nu$ value depends on the fundamental water O-H stretching frequencies and the intramolecular coupling strength, which can be calculated by the ensemble average for a subset of vibrational chromophores. The initial value can then be taken as the separation of the calculated symmetric and asymmetric stretches of the first hydration shell with the assumption that water molecules even in different subsets have $\Delta\nu$ values of similar magnitude. This assumption is validated by the analysis of the simulated symmetric and asymmetric stretches of the subsets shown in Figures S1-S7 using a value of $\Delta\nu$ ranging from 30 to 100 cm^{-1}. Therefore, our theoretical studies can guide setting the constraints of the $\Delta\nu$ value in fitting the experimental spectra.

Results and Discussion

We validate our new fitting method (equation 16) by analyzing previously reported computational and experimental spectra of hydration water around the model protein systems $LK_7\beta$ and $LE_7\beta$,[2, 14, 24] which have sequences Ac-LKLKLKL-NH_2 and Ac-LELELEL-NH_2, respectively. They fold into amphiphilic, antiparallel β-sheets at the air-water interface, making them ideal for chiral SFG studies.[25-29] The hydrophobic leucine residues (L) point into the air while the positively charged lysine (K) or the negatively charged glutamate (E) residues point into the water. It should be noted that the results presented here apply to other systems, including other proteins and even non-protein systems (e.g., DNA[1]), because the main result concerns the chiral water response rather than the response of a specific biomolecule. Therefore, the proof of the model that explains the up-down (or down-up) line shape (equation 5 and Figure 2b) remains valid regardless of the chemical identity of the biomolecules.

Lorentzian-pair-based fitting agrees with calculated chiral SFG spectra.

We start validating our model by decomposing the simulated chiral SFG spectra of water into symmetric and asymmetric O-H stretch components and then comparing them to the results of fitting the computational spectra with the new functional form (equation 16). We calculate the O-H stretch spectra of all water molecules in the first hydration shell of $LK_7\beta$ and a subset of these water molecules that are hydrogen-bonded to the peptide backbone of $LK_7\beta$ (Figure 4). The separation of symmetric and asymmetric stretch contributions is accomplished by adapting the Skinner group's inhomogeneous limit approximation approach[30-34] to calculate chiral SFG spectra. In this case, the SFG response is approximately given by

$$\chi^{(2)}_{IJK}(\omega) \approx \left\langle \sum_{a=1}^{N_{\mathrm{OH}}} \frac{\sum_{b=1}^{N_{\mathrm{OH}}} U_{ba}\alpha_b^{IJ} \sum_{b=1}^{N_{\mathrm{OH}}} U_{ba}\mu_b^{K}}{\lambda_a - \omega - \frac{i}{2\tau}} \right\rangle \tag{17}$$

where α_b^{IJ} is the IJ^{th} element of the Raman polarizability tensor of the b^{th} O-H group, μ_b^K is the K^{th} element of the transition dipole of the b^{th} O-H group, **U** is the eigenvector matrix of the exciton Hamiltonian, and λ is the eigenvalue vector of the exciton Hamiltonian. Here τ is the vibrational decay lifetime, fixed at 1.3 picoseconds in our calculations.[35] The average is over all configurations in a molecular dynamics (MD) simulation. The elements of the exciton Hamiltonian,[23, 35-40] which has vibrational frequencies on the diagonal and vibrational couplings on the off-diagonal, and the transition polarizability and dipole are computed using the Skinner group's electrostatic map relating local electric fields to these quantities, as we have used in past studies.[23, 30, 35, 37, 38, 41]

We devise a method to isolate the symmetric or asymmetric stretch components. If intermolecular couplings are neglected, the eigenvectors of the exciton Hamiltonian have the form

$$\vec{e}_a = (0 \quad 0 \quad \ldots \quad x \quad y \quad \ldots \quad 0 \quad 0) \tag{18}$$

where x and y can be both positive, both negative or of opposite signs. If x and y have the same sign, we consider the eigenvector to belong to the symmetric stretch, and the symmetric stretch response is given by

$$\chi^{(2)}_{IJK}(\omega) \approx \left\langle \sum_{a\in\text{symm}}^{N_{\text{OH}}} \frac{\sum_{b=1}^{N_{\text{OH}}} U_{ba}\alpha_b^{IJ} \sum_{b=1}^{N_{\text{OH}}} U_{ba}\mu_b^K}{\lambda_a - \omega - \frac{i}{2\tau}} \right\rangle \tag{19}$$

We calculate the asymmetric stretch response similarly by considering only those eigenvectors where x and y are of opposite sign. Notably, the asymmetric and symmetric stretch responses in the calculations are not exactly opposite because of the difference in symmetric and asymmetric frequency eigenvalues that arises from coupling.

In a recent publication, we calculated the chiral SFG response of various subsets of water molecules in the first hydration shell around $LK_7\beta$.[2] We now apply our new fitting strategy to the computed chiral response of two subsets: the entire first hydration shell and the water molecules hydrogen-bonded to the N-H groups on the protein backbone within the first hydration shell. (Similar analyses of the other subsets presented in the SI.) The chiral SFG response of these two subsets is shown in Figure 4a (purple). We chose these two subsets because they represent well the range of line shapes encountered when calculating the chiral response of various groups of water molecules around $LK_7\beta$.[2] The first hydration shell response is relatively simple (Figure 4a, left), whereas the N-H-bound water molecules produce a more complicated line shape (Figure 4a,

right). We first calculated the symmetric and asymmetric stretch chiral SFG responses (Figure 4b), as detailed above. We then fit the signals (black solid lines, Figure 4a) with the residuals of the fitting shown above Figure 4a (yellow solid lines). The signal of the first hydration shell subset is fit with a single pair of peaks (left, dashed lines, Figure 4c) and the signal of the water subset hydrogen-bonded to N-H groups is fit with two pairs (right, dashed lines, Figure 4c). We chose to fit the spectra with a minimal number of pairs to avoid overfitting.

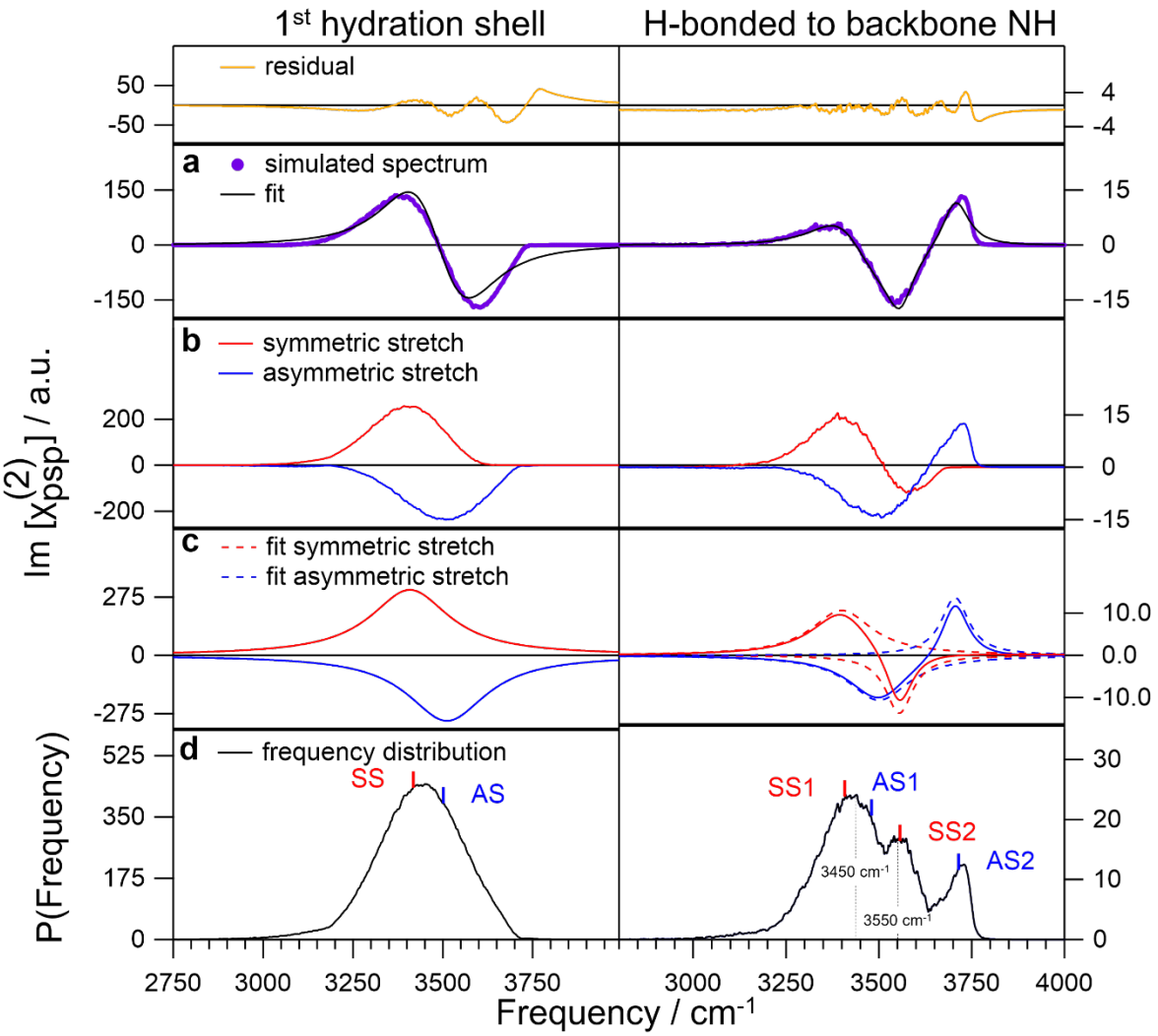

Figure 4. Lorentzian pair-based fits to computed O-H stretch chiral SFG response for the first hydration shell around $LK_7\beta$ (left) and the subset of water molecules hydrogen-bonded to N-H groups on the protein backbone (right). a) Total fits to the simulated spectra with the residual plotted at the top in yellow. b) Simulated symmetric and asymmetric stretch responses. c) Symmetric and asymmetric stretch responses (solid lines) obtained from the fit, where the dashed lines on the right indicate component peaks of two Lorentzian pairs. d) Frequency distributions obtained from the fit. The spectra in part a) were originally published in Konstantinovsky et al.[2]

Each pair of peaks is given by two Lorentzians of opposite sign, as in equation 15. In the fit to the first hydration shell spectrum, $\Delta\nu$ was taken to be 100 cm^{-1}, based on the simulated symmetric and asymmetric stretch results (Figure 4b), and A, ν, and Γ were free parameters for each pair. In the fit to the N-H-bound water spectrum, we used 100 cm^{-1} for the lower frequency pair and obtained 150 cm^{-1} for the higher frequency pair from the fitting. We identify the symmetric and asymmetric stretch components from the fit (red and blue lines, Figure 4c) using

the knowledge that the asymmetric stretch has a higher frequency than the symmetric stretch because the typical intramolecular coupling is negative.[15, 23] Accordingly, we can add all symmetric contributions (dashed red lines, Figure 4c) from the fit to yield the total symmetric response (solid red line, Figure 4c). Similarly, we can also add all asymmetric contributions (dashed blue lines, Figure 4c) to obtain the total asymmetric response (solid blue line, Figure 4c). The solid and dashed lines overlap in Figure 4c (left) because there is only one pair of water peaks. These total asymmetric and symmetric responses obtained from the fitting (solid lines, Figure 4c) appear to agree well with the total asymmetric and symmetric responses (Figure 4b) derived purely from the simulations based on the theory described in equation 19. This agreement provides evidence to support the model (Figure 2b) that explains the two-peak "up-down" (or "down-up") line shape of chiral SFG response of water molecules.

We estimate the frequency distribution of chiral water superstructures (Figure 4d) by adding the absolute values of the computationally predicted symmetric and asymmetric stretch components. We find that the first hydration shell subset has a single-peak frequency distribution. This is consistent with the IR spectrum in Figure 1b, which has a single peak around 3400 cm^{-1}, and is very similar to that of bulk water.[41] This is consistent with our previous argument that water molecules around a protein experience a similar environment to bulk water in terms of hydrogen bonding environment.[2] Whatever environment a water molecule experiences, it tries to form three to four hydrogen bonds. Furthermore, our calculations and fitting reveal that in the subset of water hydrogen-bonded to the peptide backbone N-H, the peak at the highest frequency is due solely to the asymmetric stretch component (Figure 4b-d, right). We previously argued that this high-frequency peak is due to water molecules containing one O-H group pointing into the air and another hydrogen bonded to an N-H group on the backbone.[2] We now understand that this peak is due to the asymmetric-stretch half of a pair centered at ~3650 cm^{-1} (Figure 4c, right). This interpretation indicates that the water molecules producing this pair of water peaks are not hydrogen-bond free but most likely experience some degree of hydrogen bonding with both of their O-H groups, although this hydrogen bonding is weak. Hence, the water molecules in this subset do not have O-H groups pointing directly toward the air, as that would most likely push the peak pair's central frequency above 3700 cm^{-1}. The corresponding symmetric stretch peak in the high-frequency pair (Figure 4c, right) is negative and buried in the total line shape. This analysis illustrates a subtlety of heterodyne chiral SFG – peaks can cancel and obscure each other due to

the nature of the positive- and negative-phase response. In addition, a peak in the frequency distribution (Figure 4d) does not necessarily indicate a peak *pair* center near the peak's frequency. The asymmetric stretch response may be pushed to a high frequency by intramolecular coupling effects rather than O-H groups facing into the air. Moreover, the peak in Figure 4d (right) at around 3450 cm^{-1} is primarily due to the positive symmetric stretch (red) in Figure 4b (right). The middle peak in Figure 4d (right) at around 3550 cm^{-1} is due to the negative peaks of both symmetric (red) and asymmetric (blue) stretches in Figure 4b (right).

We fit the spectra of seven other water subsets reported in Konstantinovsky et al.[2] (Figures S1-7). These subsets include (1) water associated with the backbone of $LK_7\beta$, (2) water associated with sidechains, (3) water molecules in the backbone subset but not forming hydrogen bonds with the protein, (4) water hydrogen-bonded to carbonyl groups on the backbone, (5) water forming very short hydrogen bonds with the carbonyl groups on the backbone (a distance of <1.6 Å between hydrogen and acceptor), (6) water molecules in the sidechain subset but not making hydrogen bonds to the protein, and (7) water molecules hydrogen-bonded to lysine sidechains. We have obtained very similar results. Altogether, these analyses validate our model (Figure 2b) and illustrate the advantage of the new fitting approach. Based on these analyses, we can now infer frequency distributions from chiral SFG spectra and interpret the physical meaning of peak locations.

The new model allows fitting of experimental spectra for estimating the vibrational frequency distribution.

We next apply the new fitting strategy (equation 16) to analyze our previously published experimental heterodyne chiral SFG spectra.[2, 24] The O-H-stretch peaks were identified using isotopic labeling with $H_2{}^{18}O$, which is expected to make O-H-dominated peaks red-shift by ~12 cm^{-1}.[2, 14] Peaks due to the N-H stretch were fit with conventional Lorentzians (one peak per feature). Figure 5 shows fits for experimental chiral SFG spectra of $LK_7\beta$ in H_2O (left column), $LK_7\beta$ in $H_2{}^{18}O$ (central column), and $LE_7\beta$ in H_2O (right column). The experimental spectra and their overall fits are shown in Figure 5a, the fitted Lorentzians for N-H stretches in Figure 5b, the fitted pairs of Lorentzians for O-H stretches in Figure 5c, and the estimated frequency distribution in Figure 5d. The residuals from the overall fits are plotted in yellow above Figure 5a. As seen from Figure 5a and the residuals, the fits are quite satisfactory. Also, the $H_2{}^{18}O$-induced red shifts

are clearly captured. To obtain a similarly good fit for $LK_7\beta$ using the standard approach, a total of seven Lorentzian peaks and 21 free parameters were needed (Figure S8, Tables S1-4), whereas here only 14 free parameters were used. Thus, our new fitting strategy can reduce the ambiguity of spectral analysis, improving the molecular understanding of the biomolecules and their hydration structures.

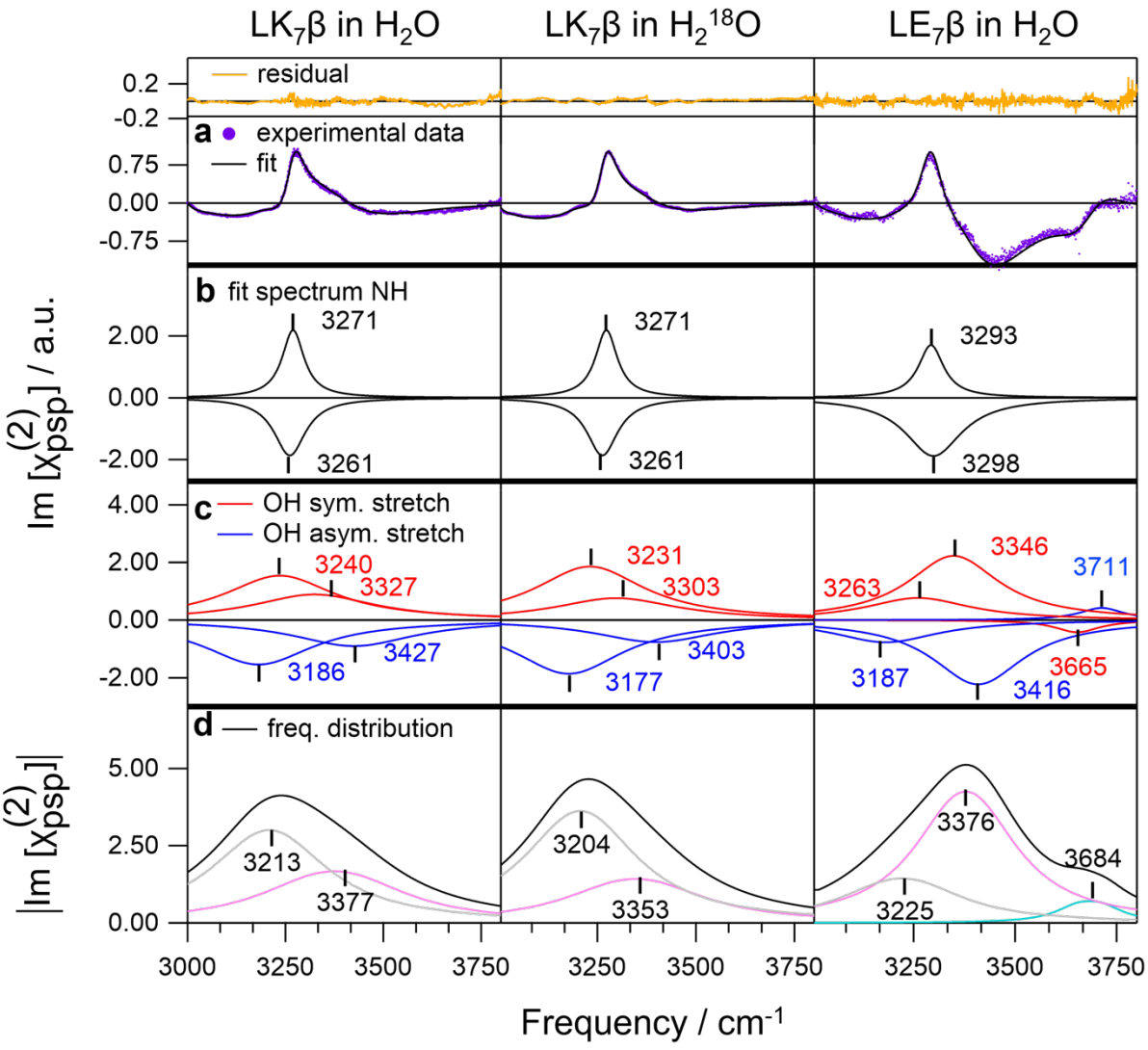

Figure 5. Fitting of experimental spectra. a) Experimental heterodyne chiral SFG spectra (purple dots) and fits (solid lines) for $LK_7\beta$ in H_2O (left column) and $H_2{}^{18}O$ (center column) and $LE_7\beta$ in H_2O (right column) with the residuals displayed at the top in yellow. b) The Lorentzian peaks used to fit the N-H stretching modes. c) The paired Lorentzian peaks used to fit the O-H symmetric (red) and asymmetric (blue) stretches. d) The O-H stretch frequency distribution (black lines) with the component frequency distributions in pink, gray, and cyan, where each labeled frequency corresponds to the center of a pair of symmetric and asymmetric stretches in part c). The spectra in part a) were previously published in Konstantinovsky et al. [2,24]

We obtain the approximate frequency distribution by adding the absolute values of the symmetric and asymmetric stretch contributions (Figure 5d). The distribution appears to be more reliable than that estimated from the conventional fit (Figure S8a). The highly jagged nature of the frequency distribution obtained using the previous conventional fit (Figure S8d) does not match the smooth nature of the calculated IR response (Figure 1b), while the frequency distribution obtained using the new fitting strategy is smoother. Isotopic labeling with $H_2{}^{18}O$ causes red shifts in the frequency distribution of the water around $LK_7\beta$, as expected. By contrast, the conventional fits show drastically different frequency distributions for H_2O and $H_2{}^{18}O$ (Figure S8), failing to reveal the expected isotopic shifts. This observation again validates the new fitting strategy for providing a molecular interpretation of chiral SFG spectra of water.

The frequency distribution of OH stretches around $LK_7\beta$ is composed of two component peaks (the first and second columns, Figure 5d), whereas the distribution around $LE_7\beta$ is composed of three component peaks (the third column, Figure 5d), including an emergent peak at a very high frequency (3684 cm^{-1}). This peak is most likely due to water molecules interacting weakly with the protein, perhaps with one OH group facing the air. We presume that such molecules also exist in the $LK_7\beta$ system. However, because the protein-hydration shell interactions are more stable in the $LK_7\beta$ system relative to the $LE_7\beta$ system, as shown previously,[24] these water molecules may contribute relatively less to the total aqueous response. It is important to note that a water molecule need not be strongly hydrogen-bonded to the protein to be part of a stable chiral hydration structure. The low frequencies in the frequency distribution around $LK_7\beta$ may correspond partially to water molecules that are *geometrically* constrained by the stable protein structure and as a result form strong hydrogen bonds with other water molecules in the first hydration shell. Hence, chiral SFG is not only a reporter of hydrogen bond strength in the first hydration shell, but also of the geometric, collective order of water molecules around the chiral biomolecular scaffolds.

The frequency distributions in Figure 5d show that $LE_7\beta$ has a significantly blue-shifted distribution of water compared to $LK_7\beta$, suggesting weaker hydrogen bonds of water surrounding the protein. This is consistent with past findings of molecular dynamics studies that $LE_7\beta$ is less stable than $LK_7\beta$ in terms of backbone hydrogen bonds.[24] Our prior experiments show that the main N-H peak is blue-shifted in $LE_7\beta$ (Figure S8). This dominant N-H contribution masks the O-H peaks, and thus the O-H stretch frequencies remained elusive in the analysis using the

conventional fitting method (Figure S8). The new fitting clearly shows that the water signal is also blue-shifted in the experimental spectra, unveiling the agreement with previously reported computational O-H stretch spectra.[42] These blue shifts of water O-H stretches and protein N-H stretches reveal that $LE_7\beta$ has a relatively lower ability to form a coherent water supramolecular structure and is less stable intrinsically. Although our previous molecular dynamics studies already demonstrated the correlation between water O-H stretches and protein N-H stretches,[24] the new fitting model allows us to reliably extract the O-H stretching frequencies of water in the first hydration shell from experiments, thereby validating the correlation. This combined experimental and computational result has a profound implication – the stability of a protein and its hydration shell can be intimately connected.

Conclusion

We have used a theoretical insight regarding the relationship between the symmetric and asymmetric stretch chiral SFG responses of water to devise a new strategy for fitting chiral SFG spectra and extracting frequency distributions. We have shown that the characteristic "up-down" or "down-up" line shape of the O-H stretch response of chiral water superstructures is due to the incomplete cancellation of opposite-phase symmetric and asymmetric stretch components. We previously showed that O-H/N-H coupling is critical to the modeling of the N-H stretch component of the SFG spectra of $LK_7\beta$ and $LE_7\beta$.[24] Thus, future investigations will need to incorporate the effects of intermolecular coupling. Although we consider only intramolecular coupling as a first approximation in this study, we have shown that the theory derived within this approximation introduces a new strategy for analyzing the experimental and computational spectra. This strategy allows for spectral interpretation to extract molecular information. The application of our theoretical model for analyzing previous experimental data has captured the isotopic shifts of water O-H stretches and revealed physical pictures of a correlation between protein stability and hydrogen-bonding interactions of water in the first hydration shell. It is possible that similar insights can be developed for other types of vibrational spectroscopy or other molecular systems, enabling more insightful analysis of experimental spectra and a better understanding of computational results.

Supporting information. Original fits to experimental data, fits to the computational spectra for seven other water subsets around $LK_7\beta$, table of fitting parameters for all experimental data fits.

Acknowledgements. The authors wish to thank Dr. Pablo Videla at Yale University for the VMD scripts to set up $LK_7\beta$ and $LE_7\beta$. This work was supported by the National Institutes of Health Grant R35 GM139449 (S.H.-S.) and the National Science Foundation Grant CHE-2108690 (E.C.-Y.Y.). D.K. was supported by these grants. T.S. was supported by CHE-2108690 (to E.C.-Y.Y.). G.J.S. gratefully acknowledges financial support for this work from the National Science Foundation (NSF-CMI 2305178, NSF-MRI-ID 2320751, NSF-CMI 2004046).

References

1. McDermott, M. L.; Vanselous, H.; Corcelli, S. A.; Petersen, P. B., DNA's Chiral Spine of Hydration. *ACS Cent. Sci.* **2017,** *3* (7), 708-714.
2. Konstantinovsky, D.; Perets, E. A.; Santiago, T.; Velarde, L.; Hammes-Schiffer, S.; Yan, E. C. Y., Detecting the First Hydration Shell Structure around Biomolecules at Interfaces. *ACS Cent. Sci.* **2022,** *8* (10), 1404-1414.
3. Perets, E. A.; Yan, E. C. Y., Chiral Water Superstructures around Antiparallel β-Sheets Observed by Chiral Vibrational Sum Frequency Generation Spectroscopy. *J. Phys. Chem. Lett.* **2019,** *10* (12), 3395-3401.
4. Yan, E. C. Y.; Perets, E. A.; Konstantinovsky, D.; Hammes-Schiffer, S., Detecting Interplay of Chirality, Water, and Interfaces for Elucidating Biological Functions. *Acc. Chem. Res.* **2023,** *56* (12), 1494-1504.
5. Perets, E. A.; Konstantinovsky, D.; Fu, L.; Chen, J.; Wang, H.-F.; Hammes-Schiffer, S.; Yan, E. C., Mirror-image antiparallel β-sheets organize water molecules into superstructures of opposite chirality. *Proceedings of the National Academy of Sciences* **2020,** *117* (52), 32902-32909.
6. Konstantinovsky, D.; Perets, E. A.; Yan, E. C.; Hammes-Schiffer, S., Simulation of the Chiral Sum Frequency Generation Response of Supramolecular Structures Requires Vibrational Couplings. *The Journal of Physical Chemistry B* **2021,** *125* (43), 12072-12081.
7. Wang, J.; Chen, X.; Clarke, M. L.; Chen, Z., Detection of chiral sum frequency generation vibrational spectra of proteins and peptides at interfaces in situ. *Proc. Natl. Acad. Sci. USA* **2005,** *102* (14), 4978-4983.
8. Stokes, G. Y.; Gibbs-Davis, J. M.; Boman, F. C.; Stepp, B. R.; Condie, A. G.; Nguyen, S. T.; Geiger, F. M., Making "Sense" of DNA. *J. Am. Chem. Soc.* **2007,** *129* (24), 7492-7493.
9. Yan, E. C. Y.; Fu, L.; Wang, Z.; Liu, W., Biological Macromolecules at Interfaces Probed by Chiral Vibrational Sum Frequency Generation Spectroscopy. *Chem. Rev.* **2014,** *114* (17), 8471-8498.

10. Fu, L.; Liu, J.; Yan, E. C. Y., Chiral Sum Frequency Generation Spectroscopy for Characterizing Protein Secondary Structures at Interfaces. *J. Am. Chem. Soc.* **2011,** *133* (21), 8094-8097.
11. Fu, L.; Wang, Z.; Yan, E. C. Y., Chiral Vibrational Structures of Proteins at Interfaces Probed by Sum Frequency Generation Spectroscopy. *Int. J. Mol. Sci.* **2011,** *12* (12), 9404-9425.
12. Moad, A. J.; Simpson, G. J., A Unified Treatment of Selection Rules and Symmetry Relations for Sum-Frequency and Second Harmonic Spectroscopies. *J. Phys. Chem. B* **2004,** *108* (11), 3548-3562.
13. Simpson, G. J., Molecular Origins of the Remarkable Chiral Sensitivity of Second-Order Nonlinear Optics. *ChemPhysChem* **2004,** *5* (9), 1301-1310.
14. Perets, E. A.; Konstantinovsky, D.; Fu, L.; Chen, J.; Wang, H.-F.; Hammes-Schiffer, S.; Yan, E. C. Y., Mirror-image antiparallel β-sheets organize water molecules into superstructures of opposite chirality. *Proc. Natl. Acad. Sci. USA* **2020,** *117* (52), 32902-32909.
15. Konstantinovsky, D.; Perets, E. A.; Yan, E. C. Y.; Hammes-Schiffer, S., Simulation of the Chiral Sum Frequency Generation Response of Supramolecular Structures Requires Vibrational Couplings. *The Journal of Physical Chemistry B* **2021,** *125* (43), 12072–12081.
16. Auer, B. M.; Skinner, J. L., Dynamical effects in line shapes for coupled chromophores: Time-averaging approximation. *J. Chem. Phys.* **2007,** *127* (10), 104105.
17. Yan, E. C. Y.; Perets, E. A.; Konstantinovsky, D.; Hammes-Schiffer, S., Detecting Interplay of Chirality, Water, and Interfaces for Elucidating Biological Functions. *Acc. Chem. Res.* **2023**.
18. Shen, Y. R., *The Principles of Nonlinear Optics*. Wiley: 2003.
19. Walker, D. S.; Richmond, G. L., Understanding the Effects of Hydrogen Bonding at the Vapor−Water Interface: Vibrational Sum Frequency Spectroscopy of H2O/HOD/D2O Mixtures Studied Using Molecular Dynamics Simulations. *J. Phys. Chem. C* **2007,** *111* (23), 8321-8330.
20. Du, Q.; Superfine, R.; Freysz, E.; Shen, Y. R., Vibrational spectroscopy of water at the vapor/water interface. *Physical Review Letters* **1993,** *70* (15), 2313.
21. Simpson, G. J., *Nonlinear Optical Polarization Analysis in Chemistry and Biology*. Cambridge University Press: Cambridge, 2017.
22. Wang, H.-F.; Velarde, L.; Gan, W.; Fu, L., Quantitative Sum-Frequency Generation Vibrational Spectroscopy of Molecular Surfaces and Interfaces: Lineshape, Polarization, and Orientation. *Annual Review of Physical Chemistry* **2015,** *66* (1), 189-216.
23. Auer, B. M.; Skinner, J. L., IR and Raman spectra of liquid water: Theory and interpretation. *J. Chem. Phys.* **2008,** *128* (22), 224511.
24. Konstantinovsky, D.; Perets, E. A.; Santiago, T.; Olesen, K.; Wang, Z.; Soudackov, A. V.; Yan, E. C. Y.; Hammes-Schiffer, S., Design of an Electrostatic Frequency Map for the NH Stretch of the Protein Backbone and Application to Chiral Sum Frequency Generation Spectroscopy. *J. Phys. Chem. B* **2023,** *127* (11), 2418-2429.
25. DeGrado, W. F.; Lear, J. D., Induction of peptide conformation at apolar water interfaces. 1. A study with model peptides of defined hydrophobic periodicity. *J. Am. Chem. Soc.* **1985,** *107* (25), 7684-7689.
26. Phillips, D. C.; York, R. L.; Mermut, O.; McCrea, K. R.; Ward, R. S.; Somorjai, G. A., Side chain, chain length, and sequence effects on amphiphilic peptide adsorption at hydrophobic and hydrophilic surfaces studied by sum-frequency generation vibrational spectroscopy and quartz crystal microbalance. *The Journal of Physical Chemistry C* **2007,** *111* (1), 255-261.

27. York, R. L.; Browne, W. K.; Geissler, P. L.; Somorjai, G. A., Peptides adsorbed on hydrophobic surfaces—a sum frequency generation vibrational spectroscopy and modeling study. *Israel Journal of Chemistry* **2007,** *47* (1), 51-58.
28. Weidner, T.; Castner, D. G., SFG analysis of surface bound proteins: a route towards structure determination. *Physical Chemistry Chemical Physics* **2013,** *15* (30), 12516-12524.
29. Fu, L.; Chen, S.-L.; Wang, H.-F., Validation of Spectra and Phase in Sub-1 cm-1 Resolution Sum-Frequency Generation Vibrational Spectroscopy through Internal Heterodyne Phase-Resolved Measurement. *J. Phys. Chem. B* **2016,** *120* (8), 1579-1589.
30. Auer, B. M.; Skinner, J. L., Dynamical effects in line shapes for coupled chromophores: Time-averaging approximation. *J. Chem. Phys.* **2007,** *127*, 104105.
31. Choi, J.-H.; Hahn, S.; Cho, M., Amide I IR, VCD, and 2d IR spectra of isotope-labeled α-helix in liquid water: Numerical simulation studies. *Int. J. Quantum Chem.* **2005,** *104* (5), 616-634.
32. Ganim, Z.; Tokmakoff, A., Spectral signatures of heterogeneous protein ensembles revealed by MD Simulations of 2DIR spectra. *Biophys. J.* **2006,** *91* (7), 2636-46.
33. Hahn, S.; Ham, S.; Cho, M., Simulation Studies of Amide I IR Absorption and Two-Dimensional IR Spectra of β Hairpins in Liquid Water. *J. Phys. Chem. B* **2005,** *109* (23), 11789-11801.
34. Belch, A. C.; Rice, S. A., The OH stretching spectrum of liquid water: A random network model interpretation. *J. Chem. Phys.* **1983,** *78* (8), 4817-4823.
35. Auer, B. M.; Skinner, J. L., Vibrational Sum-Frequency Spectroscopy of the Water Liquid/Vapor Interface. *J. Phys. Chem. B* **2009,** *113* (13), 4125-4130.
36. Schmidt, J. R.; Corcelli, S. A.; Skinner, J. L., Ultrafast vibrational spectroscopy of water and aqueous N-methylacetamide: Comparison of different electronic structure/molecular dynamics approaches. *J. Chem. Phys.* **2004,** *121*, 8887.
37. Corcelli, S. A.; Skinner, J. L., Infrared and Raman Line Shapes of Dilute HOD in Liquid H2O and D2O from 10 to 90 °C. *J. Phys. Chem. A* **2005,** *109* (28), 6154-6165.
38. Pieniazek, P. A.; Tainter, C. J.; Skinner, J. L., Interpretation of the water surface vibrational sum-frequency spectrum. *J. Chem. Phys.* **2011,** *135*, 044701.
39. Jansen, T. l. C.; Knoester, J., A transferable electrostatic map for solvation effects on amide I vibrations and its application to linear and two-dimensional spectroscopy. *J. Chem. Phys.* **2006,** *124*, 044502.
40. Jansen, T. l. C.; Dijkstra, A. G.; Watson, T. M.; Hirst, J. D.; Knoester, J., Modeling the amide I bands of small peptides. *J. Chem. Phys.* **2006,** *125*, 044312.
41. Corcelli, S. A.; Lawrence, C. P.; Skinner, J. L., Combined electronic structure/molecular dynamics approach for ultrafast infrared spectroscopy of dilute HOD in liquid H2O and D2O. *J. Chem. Phys.* **2004,** *120* (17), 8107-8117.
42. Konstantinovsky, D.; Yan, E. C. Y.; Hammes-Schiffer, S., Characterizing Interfaces by Voronoi Tessellation. *J. Phys. Chem. Lett.* **2023**, 5260-5266.